The 20S proteasome activator PA28γ controls the compaction of HP1β-linked heterochromatin

Authors:

Didier Fesquet[1][*], David Llères[2][*], Cristina Viganò[1,3], Francisca Méchali[1], Séverine Boulon[1], Robert Feil[2], Olivier Coux[1], Catherine Bonne-Andrea[1] and Véronique Baldin[1][§]

Affiliations:

1 Centre de Recherche de Biologie cellulaire de Montpellier (CRBM), University of Montpellier, CNRS, Montpellier, France

2 Institute of Molecular Genetics of Montpellier (IGMM), University of Montpellier, CNRS, Montpellier, France

3 Present address: Asst-Monza Ospedale san Gerardo, via Pergolesi 33, 20900 Monza (MB) Italy

*: These authors contributed equally to this work

§ Corresponding author: Véronique Baldin, CRBM-UMR-5237, CNRS, 1919 Route de Mende, 34293 Montpellier cedex 5, Phone: (33) 4 34 35 95 43

E-mail: veronique.baldin@crbm.cnrs.fr

Running title: PA28γ structures heterochromatin

Key words: FLIM-FRET/ Heterochromatin / HP1/ PA28γ / Proteasome.

Abstract

The nuclear PA28γ is known to activate the 20S proteasome, but its precise cellular functions remains unclear. Here, we identify PA28γ as a key factor that structures heterochromatin. We find that in human cells, a fraction of PA28γ-20S proteasome complexes localizes within HP1-linked heterochromatin foci. Our biochemical studies show that PA28γ interacts with HP1 proteins, particularly HP1β, which recruits the PA28γ-20S proteasome complexes to heterochromatin. Loss of PA28γ does not modify the localization of HP1β, its mobility within nuclear foci, or the level of H3K9 tri-methylation, but reduces H4K20 mono- and tri-methylation, modifications involved in heterochromatin establishment. Concordantly, using a quantitative FRET-based microscopy assay to monitor nanometer-scale proximity between nucleosomes in living cells, we find that PA28γ regulates nucleosome proximity within heterochromatin, and thereby controls its compaction. This function of PA28γ is independent of the 20S proteasome. Importantly, HP1β on its own is unable to drive heterochromatin compaction without PA28γ. Combined, our data reveal an unexpected chromatin structural role of PA28γ, and provide new insights into the mechanism that controls HP1β-mediated heterochromatin compaction.

Introduction

Proteasome-mediated protein degradation is a central pathway that controls the stability and the function of numerous proteins in diverse cellular processes (Collins & Goldberg, 2017). To be fully activated, the catalytic core, called the 20S proteasome, combines with different regulator/activator complexes, thereby creating a family of proteasome complexes (Rechsteiner & Hill, 2005). The best understood form of the proteasome is the 26S proteasome, composed of the 20S core proteasome and the 19S regulator, which degrades poly-ubiquitylated proteins in an ATP-dependent manner (Bard et al, 2018; Collins & Goldberg, 2017).

The homo-heptamer PA28γ (also known as REGγ or Ki antigen) constitutes another important regulator of 20S proteasome (Ma et al, 1992; Mao et al, 2008; Wilk et al, 2000). PA28γ is strictly nuclear in mammalian cells and appears essential for cell growth and proliferation, as suggested by the decrease in body size of PA28γ knockout mice (Barton et al, 2004; Murata et al, 1999). Consistent with this, a limited number of proteins, whose ubiquitin- and ATP-independent degradation is mediated by PA28γ, have been identified and many of them are involved in the control of cell proliferation such as the CKIs (p21, p19, p16) or Myc (Chen et al, 2007; Li et al, 2007; Li et al, 2015). In addition, PA28γ might play a role in nuclear organization since it has been involved in the dynamics of various nuclear bodies, including Cajal bodies (Cioce et al, 2006; Jonik-Nowak et al, 2018), nuclear speckles (Baldin et al, 2008), and promyelocytic leukemia protein bodies (Zannini et al, 2009), as well as in splicing factors trafficking (Baldin et al, 2008). A potential role of PA28γ in chromatin has been also proposed since it has been linked to chromosome stability (Zannini et al, 2008) and DNA repair (Levy-Barda et al, 2011).

It is now well established that proteasome components are associated with chromatin and enriched at specific sites in the genome (Geng & Tansey, 2012). Notably, they are specifically recruited during transcription or in response to DNA damage, thereby suggesting a direct role for chromatin-associated proteasome complexes in genomic processes (McCann & Tansey, 2014).

Chromatin compaction is necessary for genome functions. It mainly involves two distinct chromatin states. Whereas euchromatin is a relaxed state, and generally transcriptionally active, heterochromatin corresponds to the highly compacted state. Abound in repetitive sequences such as satellite repeats, transposable elements and ribosomal DNA (Janssen et al, 2018; Lippman et al, 2004; Nishibuchi & Nakayama, 2014; Saksouk et al, 2015),

heterochromatin is paramount to the stability of eukaryotic genomes. Loss of control over these repetitive regions can lead to transcriptional perturbation and DNA recombination, events all at the root of oncogenic transformation (Ayarpadikannan & Kim, 2014; Klement & Goodarzi, 2014).

Heterochromatin Protein-1 (HP1)- linked heterochromatin is associated with high levels of trimethylation of histone H3 lysine 9 (H3K9me3) (Martin & Zhang, 2005; Saksouk et al, 2015) and of histone H4 lysine 20 (H4K20me3) (Beck et al, 2012; Oda et al, 2009; Schotta et al, 2004). In this context, two proteins of the HP1 family (Nielsen et al, 2002; Thiru et al, 2004), HP1α and β, are recruited through their binding to H3K9me3, and participate to the folding of chromatin into higher-order structures (Bannister et al, 2001; Lachner et al, 2001; Machida et al, 2018; Maison & Almouzni, 2004). An intriguing point is the presence of both highly dynamic and stable HP1 populations within heterochromatin (Cheutin et al, 2003). Recent reports identify a liquid phase-like HP1 population that generates a phase transition dynamic compartment surrounding the stable chromatin-bound HP1 fraction (Larson et al, 2017; Strom et al, 2017). Such a compartmentalization mechanism may facilitate the access of proteins, and their rapid exchange, necessary for the dynamic structural changes of heterochromatin during cell cycle progression and in DNA damage response. Thus, it has been suggested that HP1 would act as a platform that selectively favors concentration of different proteins to fulfill their chromatin-related functions (Grewal & Jia, 2007). However, the mechanism by which HP1 folds chromatin-containing H3K9me3 into higher-order structures has not been fully elucidated.

By studying the localization of the 20S proteasome in human cells, we show that a fraction of PA28γ-20S proteasome complexes accumulates into HP1-rich foci. Subsequent investigations into the potential role played by PA28γ-20S proteasome complexes in these foci revealed that PA28γ is an important HP1-dependent factor that promotes heterochromatin compaction, independently of the 20S proteasome.

Results

A fraction of PA28γ-20S proteasome complexes localizes to HP1β-linked heterochromatin foci.

To investigate the subcellular location of the 20S proteasome in human cells, we established an U2OS cell line expressing an inducible alpha 4 (α4) protein, one of the subunits of the 20S proteasome (Appendix Fig S1A), fused with GFP (α4-GFP). Biochemical characterization of this cell line demonstrated that the α4-GFP subunit was correctly incorporated into the 20S and 26S proteasomes (Appendix Fig S1B-C). We found that these α4-GFP-containing complexes were proteolytically active in a proteasome activity assay, using classical fluorogenic peptides as substrates (Appendix Fig S1D).

As observed for the endogenous α4 protein (Appendix Fig S1E), ectopic α4-GFP was detected throughout the cell, with an accumulation in the nucleoplasm. However, it was also present in nuclear foci (Fig 1A), a figure that is usually not seen by immunostaining of 20S proteasome subunits. A similar confined nuclear location in foci was observed in U2OS cells expressing an α4 subunit without any tag protein, thus excluding a potential mislocalization due to the fusion with the GFP moiety (Appendix Fig S1E). Co-immunostaining experiments showed that other subunits of the 20S proteasome, such as α6, were detected in α4-GFP foci as well (Fig 1B), reflecting the presence of the entire 20S proteasome. Interestingly, in addition to the 20S proteasome, we detected PA28γ (Fig 1B), one of the activators of the 20S proteasome, but not the 19S complex, as shown by the absence of accumulation of Rpt6 subunit within α4-GFP foci (Fig 1B). Combined, these findings reveal a particular nuclear localization of PA28γ-20S proteasome complexes.

Visualization of α4-GFP in living U2OS cells, by time-lapse video microscopy, revealed that these nuclear foci were dynamic as their appearance fluctuated throughout the cell cycle (EV1-Movie). α4-GFP was diffused during mitosis, starting to assemble into foci whose number and size gradually increased during interphase. In order to define the timing of the foci formation, we determined the percentage of cells presenting α4-GFP foci at different cell cycle stages. While in asynchronously growing cells (AS), α4-GFP foci were detected in ~30% of cells, the percentage dropped to ~9 % in cells arrested at the G1 to S transition, by hydroxyurea treatment (Fig 1C, upper graph). We observed that the number of cells with α4-

GFP foci increased in mid-S phase (4h after release) to reach a percentage similar to asynchronous cells 6 hours after the release (late-S/early-G2 phases) (Fig 1C, lower graph).

An important point was to define the nature of the nuclear foci highlighted by α4-GFP expression. Among different proteins forming nuclear foci, we focused our attention on a member of the HP1 family, HP1β, reported to accumulate in heterochromatin-associated foci with a characteristic peak in late-S/early-G2 phases (Dialynas et al, 2006), a cell cycle distribution highly similar to that of α4-GFP foci. Indirect immunofluorescence was performed against HP1β protein. This revealed co-localization between α4-GFP and HP1β in these foci (Fig 1D). This finding was strengthened by immunoblot analysis of anti-PA28γ or anti-GFP pull-down experiments in U2OS-α4-GFP cell extracts, in which we detected the presence of HP1β in complexes with PA28γ and the 20S proteasome (Fig 1E). Therefore, we conclude that α4-expression allows the detection from mid-S phase to G2 phase of PA28γ-20S proteasome complexes in heterochromatin-associated nuclear foci that contain HP1β proteins.

Endogenous PA28γ and 20S proteasome complexes interact with HP1β.

Classical 20S proteasome or PA28γ immunostaining of U2OS cells only reveal a diffuse distribution within the nucleus (Appendix Fig S1E, Fig 3E and Fig 4A, respectively). Therefore, the foci evidenced above only appear upon α4 overexpression, whether the protein is tagged or not. We hypothesized that this phenomenon was due to the amplification of a natural process, which most likely occurs in normal cells and which is exacerbated upon α4 overexpression. To test this hypothesis, we asked whether the endogenous 20S proteasome and PA28γ complexes co-localize and interact with HP1 proteins. For this, we used the *in situ* Proximity-Ligation Assay (*is*-PLA), which allows the detection of interactions between two proteins only if in a close proximity to each other (less than 40 nm) in cells (Soderberg et al, 2006). Using both PA28γ and HP1β antibodies, *is*-PLA revealed a characteristic dots pattern throughout the nuclei of U2OS cells (Fig 2A, upper left panel), strongly supporting the interaction of the two proteins. Silencing of PA28γ expression with siRNAs abolished the PLA dots, demonstrating the specificity of the PLA signal (Fig 2A, lower left panel). Quantification of the number of PLA dots per nucleus (see Materials and methods) indicated on average 37 dots versus 1.4 per nucleus, in presence and absence of PA28γ respectively (Fig 2A, bar graph). Using the same approach, we monitored interactions between PA28γ and

HP1α and found an average of 15 dots per nucleus (Appendix Fig S2A), many fewer than for PA28γ/HP1β, indicating that PA28γ interacts with both HP1α and HP1β in cells. Hence, in our subsequent studies on the relationship between PA28γ and HP1 proteins, we decided to focus on HP1β. We also checked a potential co-localization/interaction between the 20S proteasome and HP1β by *is*-PLA, using antibodies against the α4 subunit of the 20S proteasome. This showed a specific co-localization/interaction between the proteins, with on average 50 dots per nucleus (Fig 2B, left panel), validated by the silencing of HP1β using siRNAs (Fig 2B, bar graph). Furthermore, immunoblot analysis of immunoprecipitation experiments, using anti-PA28γ on whole-cell extracts of U2OS cells, confirmed the interaction of HP1β with PA28γ (Fig 2C). Taken together, these results demonstrate that PA28γ and the 20S proteasome interact with the conserved heterochromatin-specific protein HP1β.

Recently, we identified an important regulator of PA28γ, the protein PIP30, which affects PA28γ interactions either positively with the 20S proteasome or negatively with coilin (Jonik-Nowak et al, 2018). We therefore asked whether PIP30 is recruited in heterochromatic foci as well and might control the interaction between PA28γ and HP1β. We found that endogenous PIP30 co-localized with α4-GFP (Fig EV1A) but that its depletion, by siRNA in U2OS-α4-GFP cells, had no influence on the number of cells with α4-GFP foci (Fig EV1B). By analyzing the interaction of PA28γ with HP1β in wild-type and PIP30 knock-out (KO-PIP30) U2OS (Jonik-Nowak et al, 2018) cells using *is*-PLA, we also observed no difference in the number of PLA-dots between PA28γ and HP1β (Fig EV1C-D). We concluded from these findings that although PIP30 is present in HP1-associated foci, it does not regulate the recruitment of the 20S proteasome into these foci, and it does not control the interaction between PA28γ and HP1β.

PA28γ controls heterochromatin compaction, independently from its interaction with the 20S proteasome.

The presence of PA28γ-20S proteasome complexes in HP1-associated heterochromatin foci and the interaction between PA28γ and HP1β prompted us to assess whether these complexes could play a role in chromatin compaction. To this end, we performed quantitative FLIM-FRET (Fluorescence Lifetime Imaging Microscopy-Förster Resonance Energy Transfer) measurements of chromatin compaction at the nanometer-scale in single living cell.

Using HeLa cells that stably co-express histone H2B-GFP and mCherry-H2B (HeLa[H2B-2FPs]), FRET was measured between fluorescent protein-tagged histones incorporated into separate nucleosomes, where an increase in FRET efficiency corresponds to an increase of chromatin compaction (Lleres et al, 2009). We first established stable CRISPR/Cas9 PA28γ knockout HeLa cell lines, expressing either H2B-GFP alone (HeLa[H2B-GFP]-KO-PA28γ) or both H2B-GFP and mCherry-H2B (HeLa[H2B-2FPs]-KO-PA28γ) (Fig 3A). We then examined the levels of nanoscale chromatin compaction in asynchronous cells by measuring the FRET efficiency in parental and KO-PA28γ cells. As shown in Figure 3B, the deletion of PA28γ led to a lower FRET efficiency in cells as illustrated on representative images of colored map of FRET efficiency, red-orange regions corresponding to high FRET were less abundant within nuclei. This effect was confirmed by the mean FRET efficiency percentage that shows a major reduction in the level of chromatin compaction compared to the wild-type (WT) HeLa[H2B-2FPs] cells. Furthermore, when PA28γ was stably re-expressed in PA28γ-depleted HeLa[H2B-2FPs] cells (two different clones were selected named KO/KI-WT#6 and # 8) at a level comparable to endogenous level (Fig EV2A), we observed that the mean FRET percentage reached a value similar to the value measured in WT cells (Fig EV2B), indicating the restoration of chromatin compaction. By comparing the FRET distribution profiles from individual nuclei in both WT and KO-PA28γ cell lines, we observed upon loss of PA28γ a marked reduction of the peak of FRET percentage corresponding to the high level of chromatin compaction (Fig 3C). In contrast, the low-FRET population corresponding to chromatin regions with the lowest degree of chromatin compaction remained unaffected. This result shows that PA28γ plays an important role in controlling chromatin compaction and potentially heterochromatin, recently shown to be organized into a nanoscale-compacted architecture *in vivo* (Lleres et al, 2017).

To confirm the results obtained from the FLIM-FRET assay and to further ask whether PA28γ regulates heterochromatin compaction, we used a previously described U2OS cell clone (F42B8) carrying *lacO* DNA repeats stably integrated within constitutive heterochromatin, at a peri-centromeric region (Jegou et al, 2009). This *lacO* array forms a single heterochromatic locus that can be visualized in cells following the transient expression of the GFP-LacI construct. To examine the effect of PA28γ depletion, we first transfected these cells with si-RNAs PA28γ (si-PA28γ) or luciferase (si-Luc), and then transiently transfected them with GFP-LacI construct. The efficiency of si-PA28γ was verified by immunoblot (Fig 3D) and changes in heterochromatin compaction state were monitored 48

hours post-transfection by fluorescence microscopy (Fig 3E). Targeting GFP-LacI to the LacO repeat array allowed us to detect the condensed state of the locus. It appeared as a small dot with a surface area that was not significantly affected by the transfection of si-Luc (0.44 ± 0.011 μm^2 vs 0.37 ± 0.052 μm^2 in control cells). In contrast, upon PA28γ knock-down we observed a significant increase of the GFP-LacI dot surface area (0.64 ± 0.014 μm^2). This corresponds to an expansion of the surface area occupied by the LacO DNA repeat (1.73 fold as compare to control cells) due to heterochromatin decompaction (Fig 3E-F). These data are consistent with the loss of compaction affecting heterochromatin in the absence of PA28γ as observed in the FLIM-FRET assay.

We next investigated the involvement of the 20S proteasome itself in heterochromatin compaction. For this, we used a mutant of PA28γ deleted from its last C-terminal 14 amino acids (called ΔC), which is unable to bind and therefore to activate the 20S proteasome (Ma et al, 1993) (Zannini et al, 2008). We stably expressed this mutant in HeLa[H2B-2FPs]-KO-PA28γ cells (named KO/KI-ΔC) at an expression level comparable to that observed in WT cells (Fig EV2C). The inability of this PA28γ-mutant to bind the 20S proteasome was confirmed by co-immunoprecipitation and immunoblot analyses on total cell extracts of HeLa[H2B-2FPs]-WT, -KO-PA28γ, -KO/KI-WT and -KO/KI-ΔC cells, treated (Fig 3G) or not (Fig EV2D) with a catalytic inhibitor of the 20S proteasome (MG132) known to increase the association between PA28γ and 20S proteasome (Welk et al, 2016). As illustrated in figures 3G and EV2D, the 20S proteasome was detected by the presence of its α4 subunit in PA28γ pull-downs of HeLa[H2B-2FP] cells WT and KO/KI-WT cell extracts, but not of KO/KI-ΔC and KO-PA28γ cell extracts. Chromatin compaction was then examined by measuring the FRET efficiency in living asynchronous cells. FRET efficiency was calculated and its spatial distribution throughout nuclei was depicted (Fig 3H, left panel). Interestingly, we found that the expression of PA28γ-ΔC mutant restored the chromatin compaction in PA28γ-KO cells leading to a FRET efficiency value (24.7%) similar to the one observed in WT cells (23.03%) (Fig 3H, bar graph). These results demonstrate that the compaction of heterochromatin requires PA28γ, but not its interaction with the 20S proteasome.

HP1β is required to recruit PA28γ to heterochromatin foci.

We then wondered whether HP1β is responsible for the recruitment of PA28γ and 20S proteasome to heterochromatin foci. To test this possibility, we used the U2OS cells

expressing α4-GFP. After depletion of HP1β by siRNA in these cells (Fig 4A and Appendix Fig S2B), we observed a significant decrease in the percentage of cells containing α4-GFP foci (~14%) compared to the control cells (~36%) (Fig 4A, bar graph). Importantly, we noted that PA28γ was not recruited to identifiable nuclear foci in the absence of HP1β as well. This indicates that HP1β is required for the recruitment of PA28γ and the 20S proteasome to heterochromatin-associated foci.

We then investigated whether PA28γ and the 20S proteasome were recruited into heterochromatin foci together or independently from each other. For this, we used si-PA28γ in U2OS-α4-GFP cells (Fig 4A) or transient expression of α4-GFP in U20S cells and a U2OS-KO-PA28γ cell line (Jonik-Nowak et al, 2018) (Fig 4B and Appendix Fig S2C). In both experimental setups, we observed in the absence of PA28γ a significant decrease in the percentage of cells with α4-GFP foci compared to control cells (Fig 4A-B). These observations indicate that the recruitment of the 20S proteasome to heterochromatin foci requires the presence of PA28γ.

PA28γ depletion does not modify HP1β dynamics, but affects H4K20 methylation.

Since we found that a fraction of PA28γ and the 20S proteasome interacts with HP1β and localizes in heterochromatin foci, we next evaluated the consequences of depleting PA28γ on HP1β-associated nuclear foci. We observed no significant difference with either endogenous HP1β or ectopically expressed GFP-HP1β proteins by comparing WT and KO-PA28γ U2OS cells (Fig 4C). To consolidate this result, we examined the levels of H3K9me3, a hallmark modification for HP1 binding and heterochromatin formation (Maison & Almouzni, 2004; Saksouk et al, 2015; Trembecka-Lucas et al, 2013). No change in the steady-state level of H3K9me3 was observed in KO-PA28γ cells compared to WT cells (Fig 4D). We also analysed whether HP1β mobility is altered in absence of PA28γ within HP1 β nuclear foci. For that, we measured the mobility of GFP-HP1β by fluorescence recovery after photobleaching (FRAP) in U2OS-WT or -KO-PA28γ cells (Fig EV3). We observed that the mobile fraction of HP1β (96%) was identical in both cell lines, and that the dynamics of HP1β, evaluated by the measure of the half-time recovery ($\tau_{1/2}$) was unchanged in WT- and KO-PA28γ-U2OS cells ($\tau_{1/2} = 0.49 \pm 0.17$ and 0.46 ± 0.16 s, respectively). Together, these results indicate that PA28γ does not control the location and dynamics of HP1β in heterochromatic foci.

Besides the recruitment of HP1 proteins via histone H3K9 tri-methylation, methylation of histone H4 on lysine 20 (H4K20me) has been shown to be important for chromatin compaction (Shoaib et al, 2018). Since tri-methylation of histone H4 (H4K20me3) is an evolutionarily conserved mark of heterochromatin (Balakrishnan & Milavetz, 2010; Beck et al, 2012; Schotta et al, 2004), we tested whether PA28γ regulates this heterochromatic modification. Immunoblot analysis of total cell extracts showed that PA28γ depletion led to a decrease (~20 %) in the steady-state level of H4K20me3 (Fig 4E). In the present context, this result was particularly interesting since it has been recently suggested that HP1β mediates a direct functional link with H4K20me3 (Bosch-Presegue et al, 2017). As H4K20me3 depends on the mono-methylation of histone H4 lysine K20 (H4K20me1) (Tardat et al, 2007), we also analyzed the steady-state of H4K20me1. Immunoblot analysis revealed a strong reduction of H4K20me1 (~40 %) (Fig 4E). These data suggest that PA28γ participates to the regulation of histone H4K20 methylation states necessary for heterochromatin compaction (Shoaib et al, 2018). Altogether our results indicate that PA28γ acts downstream of HP1β.

PA28γ is required for HP1 to mediate heterochromatin compaction.

To further analyze the real contribution of PA28γ to chromatin compaction, we performed siRNAs mediated depletion of both PA28γ and HP1β proteins and analyzed the effects on chromatin compaction levels in HeLa^H2B-2FPs cells by FLIM-FRET. The efficiency of the siRNAs knockdown was verified by immunoblot analyses, which showed that the expression level of each protein was drastically reduced (Fig 5A). We then examined the effects of the depletion of PA28γ, of HP1β and of both proteins together on FRET efficiency. Determination of the mean FRET efficiency values showed a marked decompaction of chromatin upon PA28γ knock-down, that was strikingly more pronounced than the decompaction observed upon HP1β depletion (Fig 5B). As illustrated in figure 5C (left panel), the heterogeneous FRET efficiency map observed throughout nuclei in control si-Luc treated cells was highly altered upon si-PA28γ treatment alone: the highest FRET efficiency regions (red-orange regions) clearly decreased to lower values of FRET efficiency (blue-green regions), as it was observed in KO-PA28γ cells. When the FRET efficiency profiles was analyzed, we noted that the transfection of the si-Luc only (blue curve) caused an increase of the high-FRET population (Fig 5C right panel) as compare to parental cells, confirmed by determination of the mean FRET efficiency (Appendix Fig S2D). Interestingly, analysis of the FRET distribution profiles revealed a less pronounced decompaction of the

chromatin with remaining high FRET values upon si-HP1β depletion than upon si-PA28γ depletion (Fig 5C right panel, compare red curve to the black one). This effect could be attributed to the presence of HP1α and /or to the redundancy of the HP1 isoforms (HP1a/β) in regulating chromatin compaction (Bosch-Presegue et al, 2017). Intriguingly, we noted that unlike in KO-PA28γ cells, PA28γ knock-down by siRNA increased the proportion of very low FRET efficiency (between 1-3 %), as well as upon si-HP1β but less marked. This difference could be explained by potential compensatory mechanisms developed by the PA28γ-KO cell during establishment. Moreover, importantly the concomitant depletion of PA28γ and HP1β did not change the FRET distribution profile observed upon PA28γ-depletion alone.

Taken together, our results show that PA28γ is a key factor required for heterochromatin compaction at the nanometer scale level, and that it acts downstream of HP1β (Fig 6).

Discussion

HP1 proteins regulate the establishment and maintenance of heterochromatin organization, but the mechanism by which HP1 proteins structure this H3K9me3-marked chromatin has not been fully elucidated. A key finding of this study is that PA28γ, a nuclear activator of the 20S proteasome, is an essential factor in the HP1β-dependent process of chromatin compaction. We show that recruitment of PA28γ to heterochromatin foci occurs via its association with HP1β. Our study shows that PA28γ acts downstream of HP1β, and seems to mediate its function in heterochromatin compaction by regulating the levels of H4K20 methylation.

Under which circumstances PA28γ and the 20S proteasome are recruited via HP1β to heterochromatin foci? We found that, in human cells, the PA28γ-20S proteasome complex gradually concentrates into foci through mid to late S phase to G2 phase. This is reminiscent to the accumulation of newly-synthetized HP1β into constitutive heterochromatin foci whose formation has been shown to require passage through the S-phase (Dialynas et al, 2006). Considering this point, it is tempting to hypothesize that, following the progression of the replication fork and after PA28γ recruitment by HP1β, PA28γ might regulate the re-establishment of modifications on the newly incorporated histones on each of the daughter DNA strands. In favor of this hypothesis, no variation of the steady-state levels of H3K9me3, necessary for HP1β binding was observed. Rather, we find that depletion of PA28γ results in a significant decrease in H4K20me1, and to a lesser extent also of H4K20me3. This last point argues for a possible role of PA28γ in the regulation of these histone marks, by potentially facilitating the function of the lysine methyltransferase PR-Set7, responsible for H4K20 mono-methylation, and whose activity starts to peak in late-S phase/G2 (Beck et al, 2012). Of course, such a hypothesis does not exclude that PA28γ functions in other processes in which partial dissociation and modification of nucleosomes occur.

The fact that the 20S proteasome, that bears the proteolytic activities, is not necessary for PA28γ-mediated chromatin compaction precludes any direct regulation of this process by PA28γ-dependent proteolysis event. Thus, one possibility that needs to be explored in future studies is whether, once recruited by HP1β, PA28γ might control H4K20me1 through Pr-Set7 recruitment, or by maintaining H4K20me1 methylation, and/or by recruiting complexes involved in chromatin remodeling. It is interesting to note that the PA28γ interactome contains two major interactors BRD9 and SMARCA4 (BRG1) (Jonik-Nowak et al, 2018), which are two subunits of a newly defined ATP-dependent chromatin remodeling complex

(ncBAF for non-canonical BAFs) (Alpsoy & Dykhuizen, 2018). The physiological significance of these interactions in the new function of PA28γ in heterochromatin compaction remains to be determined.

Interestingly, recent studies show that HP1 has the capacity to form liquid-like droplets resulting from a liquid-liquid phase separation (LLPS) mechanism (Larson et al, 2017; Strom et al, 2017). This could facilitate the enrichment and rapid exchange of various proteins required for heterochromatin compaction, and might thus stimulate PA28γ's interactions with other proteins required for heterochromatin compaction. In this context, it is important to underline that PA28γ is involved in the dynamics of various membrane-less nuclear bodies (Baldin et al, 2008; Cioce et al, 2006; Jonik-Nowak et al, 2018; Zannini et al, 2009), also considered to be liquid-like protein droplet organelles (Erdel & Rippe, 2018; Sawyer et al, 2019).

The reason behind the recruitment of 20S proteasome in heterochromatin-associated foci, is still an intriguing open question, since its interaction with PA28γ is not required for PA28γ-mediated chromatin compaction? In fission yeast, the 26S proteasome (i.e.: 20S proteasome associated to the 19S regulator complex) is involved in the control of heterochromatin spreading at centromeres (Seo et al, 2017), and in the regulation of facultative heterochromatin formation (Seo et al, 2018). Whether PA28γ-20S proteasome complexes are involved in this function in mammalian cell remains to be investigated. One other possibility, in line with a possible link with LLPS droplet organelle formation (Sawyer et al, 2019), is that the recruitment of PA28γ-20S proteasome complexes into liquid-like HP1β droplets could constitute a reservoir of active proteasome that can rapidly act upon DNA damage occurring in the heterochromatic environment. Different results support this possibility. First, PIP30, which positively regulates PA28γ-20S proteasome association (Jonik-Nowak et al, 2018), is present with PA28γ and the 20S proteasome in HP1β foci (this study). Second, PA28γ-20S proteasome complexes are involved in the cellular response to DNA double-strand breaks (DSBs), in which PA28γ is required for the rapid mobilisation of the 20S proteasome at DNA damage sites (Levy-Barda et al, 2011). It also contributes to the repair-pathway choice, since its depletion causes a marked elevation in homologous recombination (HR) and a moderate reduction in non-homologous end-joining repair (NHEJ) (Levy-Barda et al, 2011). Finally, HP1β was also shown to be recruited at DSBs sites and to help to initiate the DNA damage response (DDR) by promoting chromatin changes (Ayoub et al, 2008; Bartova et al, 2017; Luijsterburg et al, 2009). It is therefore possible that the 20S proteasome recruited via PA28γ

into HP1β-heterochromatin foci serves as a reservoir that can be quickly mobilized at DNA damage sites to fulfil it proteolytic functions. It would therefore be interesting to investigate whether the mobilization of PA28γ to DNA damage sites also occurs via HP1β.

An appealing hypothesis, supported by our data, is that most of the functions identified so far for PA28γ such as maintenance of chromosomal stability (Zannini et al, 2008), DNA repair (Levy-Barda et al, 2011) and control of rDNA transcription (Sun et al, 2016), most likely occur as a result of its role in heterochromatin compaction. Although much remains to be understood regarding PA28γ biological functions in this process, our results implicate PA28γ as an important new factor required for HP1-mediated heterochromatin compaction.

Materials and methods

Plasmids

Human cDNA encoding the full-length of 20S proteasome subunit α4 (*PSMA7*), with or without final stop codon, was PCR amplified from a human fibroblast cDNA library and inserted into pcDNA$_3$ or pML1-EGFP (Baldin et al, 2008). The cDNA coding α4-EGFP was then inserted into pTRE2 vector (Clontech). Human HP1β (*CBX1*) cDNA was PCR-amplified from pDONR223 (provided by the Montpellier Genomic Collections facility, IGMM, Montpellier, France) and cloned into pEGFP-C1 (Clontech). For Cas9-mediated gene disruption, guide RNA (GGAAGTGAAGCTCAAGGTAGCGG) targeting PA28γ (*PSME3*) was selected using ChopChop (https://chopchop.rc.fas.harvard.edu/index.php) and oligonucleotides were subcloned in pMLM3636 (gift from Keith Joung, Addgene, plasmid # 43860) and pUC57-U6 (gift from Edouard Bertrand's laboratory, IGMM, Montpellier, France). For rescue experiments, PA28γ ORF WT or delta C-terminal 14 amino acids (called ΔC) were cloned in pSBbi-Pur (gift from E. Kowarz addgene plasmid #60523) according to (Kowarz et al, 2015). The resulting vector was co-transfected with pCMV(CAT)T7-SB100 (gift from Zsuzsanna Izsvak Addgene plasmid # 34879) in recipients cells and puromycin resistant single colonies selected for re-expression of PA28γ WT or ΔC proteins. pEGF-LacI (Jegou et al, 2009) was a generous gift of Karsten Rippe (DKFZ, Heidelberg, Germany).

Antibodies

The following antibodies were used at 1:1000 dilution for immunoblotting and 1-3 μg/ml for immunuprecipitation: anti-PA28γ (rabbit polyclonal BML-PW8190), anti-α4 (1:2000), anti-α6 (1:2000), and anti-Rpt6/Sug1 (mouse monoclonal, BML-PW8120, BML-PW8100 and BML-PW9265, ENZO Life Sciences, respectively), anti-PA28γ (mouse monoclonal, 611180, BD Transduction), anti-HP1α (rabbit polyclonal, 2616S, Cell Signaling), anti-HP1β (rabbit monoclonal (D2F2), 8676S, Cell signaling; mouse monoclonal (1MOD-1A9) 39979, Active Motif), anti-PIP30 (Jonik-Nowak et al, 2018), anti-GFP (mouse monoclonal (Clone 7.1), 11814460001, ROCHE, Sigma), anti-β-actin (rabbit monoclonal, 13E5, Cell Signaling), anti-H3K9me3 (mouse monoclonal (2AG6F12 H4), 39285, Active Motif), anti-H3 (rabbit polyclonal, ab1791, Active Motif), anti-H4K20me1 (rabbit polyclonal, #9724, Cell Signaling Technology), anti-H4K20me3 (rabbit monoclonal, #5737, Cell Signaling Technology), anti-α -tubulin (mouse monoclonal, T9026, Sigma, 1:6,000). Fluorescent secondary antibodies

conjugated either to AlexaFluor 488, 594 and 680 (1:1,000), or to DyLight 680 and 800 (1:10,000) were purchased from Molecular Probes and ThermoFisher Scientific, respectively. Secondary antibodies conjugated to HRP were purchased from Bio-Rad SA (1:10,000) and GFP-TRAP-A® beads (ChromoTek).

Cell culture, transfections, synchronization and FACS analysis

HeLa (CCL-2) and U2OS (HTB-96) cells, obtained from ATCC, were grown in DMEM (Lonza) containing 4.5 g/L glucose, 10% heat inactivated fetal bovine serum (Biowest), 2mM glutamine, 100 U/ml penicillin and 10 µg/ml streptomycin (Lonza). U2OS Tet-off stable inducible cell line, expressing α4-EGFP, was established as previously described (Theis-Febvre et al, 2003) and cultured in medium supplemented with 250 mg/ml G418 (Sigma), 200 mg/ml hygromycin B (Calbiochem) and 2 mg/ml tetracycline (Sigma). α4-EGFP expression was induced for 24 to 36 hours in absence of tetracycline. U2OS-LacO (F42B8) cells (a generous gift of K. Rippe, DKFZ, Heidelberg, Germany) were grown in the same media that U2OS but containing G418 (500 mg/ml) (Jegou et al, 2009). Establishment and characterization of parental HeLa$^{H2B-GFP}$ and HeLa$^{H2B-2FPs}$ (H2B-GFP and mCherry-H2B) cell lines were previously described (Lleres et al, 2009). Of note after thawing cells are cultured one week before seeding for all experiments.

For transient PA28γ, HP1β and PIP30 knock-down, U2OS and/or HeLa (H2B-GFP or 2FPs) cells were transfected with 20 nM of Luciferase targeting siRNA (siLuc, 5'-CGTACGCGGAATACTTCGA-3') used as negative control, or PA28γ (*PSME3*), HP1β (*CBX1*) and PIP30 (*FAM192A*) targeting siRNA (siPA28γ: 5'-GAAUCAAUAUGUCACUCUA-3'; siHP1β: 5'-AGGAAUAUGUGGUGGAAAA-3'; siPIP30: On target plus SMART pool: L-014528-01-0005) purchased from Eurofins Genomics or Darmacon, using Lipofectamine RNAiMAX (Thermo Fisher Scientific) and examined after 2 days. When indicated, cells were transiently transfected with 0.5 µg/ml DNA using JetPEI^{TM} (Ozyme), according to the manufacturer's instructions and analyzed after one day. Stable U2OS (Jonik-Nowak et al, 2018), HeLa$^{H2B-GFP}$- and HeLa^{2FPs}-KO-PA28γ cell lines were generated by co-transfection of PSME3/PA28γ sgGuide and pX459 vectors (a gift from Feng Zhang Addgene plasmid # 62988), and cells were selected with puromycin (1 µg/ml). Single clones were then expanded and analyzed by western blotting using PA28γ antibodies. Synchronization of cells at G1/S phases transition was performed by Hydroxyurea treatment (10 mM, Sigma) for 16 hours. For Fluorescence-activated cell sorting (FACS)

analysis, cells were fixed with 70% ethanol and conserved at -20°C. Before analysis, cells were washed with PBS, resuspended in PBS containing RNAse A (1 mg/ml, Sigma) and propidium iodide (10 μg/ml, Sigma) and incubated for 30 min at room. Samples were run on a FACS Calibur (Becton-Dickinson) and data analysis was performed using CellQuest Pro software (Beckton-Dickinson).

FLIM-FRET Microscopy.

FLIM-FRET data were acquired with a Zeiss LSM 780 laser scanning microscope coupled to a 2-photon Ti:Saphire laser (Chameleon Ultra II tunable 680–1080 nm, Coherent) producing 150-femtosecond pulses at 80 MHz repetition rate and a Time Correlated Single Photon Counting (TCSPC) electronics (SPC-830; Becker & Hickl GmbH) for time-resolved detection. Enhanced green fluorescent protein (EGFP) and mCherry fluorophores were used as a FRET pair. The two- photon excitation laser was tuned to 890 nm for selective excitation of the donor fluorophore. LSM780 microscope is equipped with temperature- and CO_2-controlled environmental black wall chamber. Measurements were acquired in live cells at 37 °C, 5% CO_2 with 63x/1.4 oil Plan-Apochromat objective lens. A short-pass 760-nm dichroic mirror was used to separate the fluorescence signal from the laser light. Enhanced detection of the emitted photons was afforded by the use of the HPM-100 module (Hamamatsu R10467-40 GaAsP hybrid PMT tube). The FLIM data were processed by the SPCimage software (Becker & Hickl GmbH).

FLIM-FRET analysis

FLIM-FRET experiments were performed in HeLa cells stably expressing H2B-GFP alone (HeLa[H2B-GFP]) or with mCherry-tagged histone H2B (HeLa[H2B-2FPs]). Cells were seeded at 5.10^4 in Fluorodish 35 (FD35-100, World Precision Instruments). For siRNA experiments, 24 hours after seeding, cells were transfected with 20 nM of siRNA (against Luciferase, or PA28γ or HP1β) and FLIM-FRET experiments were performed 48 hours later. 30 min prior imaging, culture medium was changed to complete DMEM medium without phenol red. An acquisition time of 90 s was set up for each FLIM experiment. The analysis of the FLIM measurements was performed by using the SPCImage software (Becker & Hickl, GmbH). Because FRET interactions cause a decrease in the fluorescence lifetime of the donor molecules (EGFP), the FRET efficiency was calculated by comparing the FLIM values obtained for the EGFP donor fluorophores in the presence (HeLa[H2B-2FPs]) and absence (HeLa[H2B-GFP]) of the mCherry acceptor fluorophores. FRET efficiency (E FRET) was derived by applying the following equation:

E FRET = 1- (τDA / τD) at each pixel in a selected region of interest (nucleus) using SPCImage software. τDA is the mean fluorescence lifetime of the donor (H2B-EGFP) in the presence of the acceptor mCherry-H2B in HeLa[H2B-2FPs] cells and τD is the mean fluorescence lifetime of H2B-EGFP (in the absence of acceptor) in HeLa[H2B-GFP] cells. The FRET distribution curves from nuclei were displayed from the extracted associated matrix using SPCImage and then normalized and graphically represented using Excel and GraphPad Prism software. For each experiment, FLIM was performed on multiple cells from several independent experiments (see figure legends).

Time-lapse video microscopy

U2OS-α4-GFP cells seeded on a-6-well plate were induced to expressed α4-GFP 24 hours before and imaged on an Olympus IX83 microscope with a 40x objective and equipped with Andor Zyla 4.2 sCMOS camera (van Dijk et al, 2018). Both systems were driven by Metamorph software. Image were then processed with the imageJ package and saved in Avi Format Schneider, C.A., (Schneider et al, 2012).

Immunofluorescence and is-PLA assays

Cells on coverslips were fixed in 3.7% paraformaldehyde/PBS at room temperature then permeabilized with 0.25% Triton-X100 in PBS, 5 min, followed by an incubation in cold methanol (100%) 10 min at -20°C. After washes with PBS, cells were blocked with 1% FCS/PBS for 15 min. Incubation with primary antibodies (anti-PA28γ 1:6,000 for BML-PW8190 or 1:1,000 for 611180); anti-α4, anti-α6, and anti-Rpt6/Sug1 (1:4,000 BML-PW8120, 1:1,000 BML-PW8100 and 1:1,000 BML-PW9265, respectively); anti-HP1α (1:1,000, 2616S) used in *is*-PLA; anti-HP1β (1:1,000 8676S and 1MOD-1A9); anti-PIP30 (1:2,000 (Jonik-Nowak et al, 2018) was carried out at 37°C for 1 hour in a humidified atmosphere. After washes, cells were incubated with Alexa-Fluor conjugated secondary antibodies for 40 min at RT. DNA was stained with 0.1 μg/ml DAPI (4,6-diamidino-2phenylindole, dihydrochloride, Sigma) solution 5 min at RT, cells were washed twice in PBS and finally once in H$_2$O. Coverslips were mounted on glass slides using ProLong Gold antifade reagent (Thermo Fisher Scientific).

For *in situ* proximity ligation assays (*is*-PLA), cells on coverslips were fixed and permeabilized as above. Coverslips were then blocked in a solution provided by the Duolink® kit (Sigma). Cells were then incubated with mentioned antibodies as described above.

Duolink® *In Situ* PLA Probe Anti-Rabbit MINUS and Anti-Mouse PLUS and Duolink® *In Situ* Detection Reagents (Sigma) were used, according to the manufacturer's instructions.

Z-stacks images were acquired with 63X/1.32 NA or 100X/1.4 NA oil immersion objective lenses using a DM 6000 microscope (Leica). Microphotographs were taken with a 12-bit CoolSnap HQ2 camera. Images were acquired as TIF files using the MetaMorph imaging software (Molecular Devices). For PLA dots quantitative analyzes, Z-stacks were acquired every 0.3 μm (Z step) with a range of 6-7.5 μm. The number of PLA-dots and the size of GFP-LacI dots were detected with ImageJ (1.49v). Specific macros have been created to automatically quantify these different parameters. The script allows to create a mask of DAPI image to isolate the nucleus of each cell and create a maximum intensity projection (MIP) of the Z-stacks or the image. The mask is used in the MIP to count the number of PLA-dots of each nucleus via an appropriate thresholding. The "Analyze Particles" tool of ImageJ was used to calculate the size of each GFP-LacI dots.

Fluorescence recovery after photobleaching

For FRAP experiments, U2OS cells (parental or PA28γ knock-out) grown in Fluorodish 35 were transfected with 0.2 μg of pEGFP-HP1β. Twenty-four hours post-transfection, FRAP was performed on a Leica TCS SP5 II laser microscope, using the FRAP wizard function of Leica LAS software. For FRAP, the 488 nm line of an Argon laser was used in combination with a Leica 63x/1.4 oil Apo objective lens for bleaching GFP fluorophores, and observation of their fluorescence recovery. A small region inside nucleus corresponding to GFP-HP1β bright foci was selected for photobleaching. Briefly, 25 prebleach images were recorded every 0.041 s followed by a bleach pulse of four iterations with the 488 nm laser line sets at 100% laser power. After bleaching, 600 postbleach images were collected every 0.04 s. The fluorescence intensities in the bleached and non-bleached nucleus regions, and background before and after laser photobleaching, were extracted using the Leica software. Then, the quantitative analysis of FRAP raw experimental data was performed by using easyFRAP application software (Rapsomaniki et al, 2012).

Immunoprecipitation and immunoblotting

For immunoprecipitation of GFP-fusion or endogenous proteins, cells were lysed in lysis buffer (50 mM Tris-HCl, pH 8.0, 100 mM NaCl, 5 mM MgCl$_2$, 0.5 mM EDTA, 1 mM ATP, 1 mM DTT, 10% Glycerol, 0.5% IGEPAL CA630, 0.3% Triton X-100) for 20 min at 4°C. Lysates were clarified by centrifugation for 10 min at 10,000 x g and the protein

concentration of the supernatant was determined using BSA as a standard (CooAssay protein dosage reagent, Interchim). Total lysate (200 μg) was pre-cleared for 30 min, and immununoprecipitations were performed using either GFP-TRAP beads or indicated antidodies and protein A or G magnetic beads (Dynal, Lake Success, NY) for 2 hours at 4°C with constant gentle stirring. After several washes, bead pellets were boiled in 2X Laemmli buffer, separated by SDS-PAGE and immunoblotting. Note that, i) for co-immunoprecipitation of α4-GFP and HP1β proteins, cells were homogenized in a modified lysis buffer (50 mM Tris-HCl, pH 7.5, 150 mM NaCl, 5 mM $MgCl_2$, 1% IGEPAL CA630, 0.5% DOC, 0.1% SDS, 1 mM DTT, 5 mM EDTA, 50 mM NaF and 1 mM Na_3VO_4) in presence of complete EDTA free protease inhibitor cocktail (Life Science-Roche) in the same conditions, and ii) immunoblotting of whole-cell extracts were performed on cells directly lysed in 2X Laemmli sample buffer.

Statistics

Error bars are SD unless otherwise noted. Different tests were used to determine significance and noted in the legend.

Author contribution

VB conceived the project and supervised the study. DF, DL, CV, SB, CBA, and VB performed experiments and analyzed data. FM generated reagents. OC and RF provided conceptual advice on study and interpretation of the data. CBA and VB wrote the article with input from all of the authors.

Conflict of interest

The authors declare that they have no conflict of interest.

Acknowledgements

Funding

References

Alpsoy A, Dykhuizen EC (2018) Glioma tumor suppressor candidate region gene 1 (GLTSCR1) and its paralog GLTSCR1-like form SWI/SNF chromatin remodeling subcomplexes. *J Biol Chem* 293: 3892-3903

Ayarpadikannan S, Kim HS (2014) The impact of transposable elements in genome evolution and genetic instability and their implications in various diseases. *Genomics Inform* 12: 98-104

Ayoub N, Jeyasekharan AD, Bernal JA, Venkitaraman AR (2008) HP1-beta mobilization promotes chromatin changes that initiate the DNA damage response. *Nature* 453: 682-686

Balakrishnan L, Milavetz B (2010) Decoding the histone H4 lysine 20 methylation mark. *Crit Rev Biochem Mol Biol* 45: 440-452

Baldin V, Militello M, Thomas Y, Doucet C, Fic W, Boireau S, Jariel-Encontre I, Piechaczyk M, Bertrand E, Tazi J, Coux O (2008) A novel role for PA28gamma-proteasome in nuclear speckle organization and SR protein trafficking. *Mol Biol Cell* 19: 1706-1716

Bannister AJ, Zegerman P, Partridge JF, Miska EA, Thomas JO, Allshire RC, Kouzarides T (2001) Selective recognition of methylated lysine 9 on histone H3 by the HP1 chromo domain. *Nature* 410: 120-124

Bard JAM, Goodall EA, Greene ER, Jonsson E, Dong KC, Martin A (2018) Structure and Function of the 26S Proteasome. *Annu Rev Biochem* 87: 697-724

Barton LF, Runnels HA, Schell TD, Cho Y, Gibbons R, Tevethia SS, Deepe GS, Jr., Monaco JJ (2004) Immune defects in 28-kDa proteasome activator gamma-deficient mice. *J Immunol* 172: 3948-3954

Bartova E, Malyskova B, Komurkova D, Legartova S, Suchankova J, Krejci J, Kozubek S (2017) Function of heterochromatin protein 1 during DNA repair. *Protoplasma* 254: 1233-1240

Beck DB, Oda H, Shen SS, Reinberg D (2012) PR-Set7 and H4K20me1: at the crossroads of genome integrity, cell cycle, chromosome condensation, and transcription. *Genes Dev* 26: 325-337

Bosch-Presegue L, Raurell-Vila H, Thackray JK, Gonzalez J, Casal C, Kane-Goldsmith N, Vizoso M, Brown JP, Gomez A, Ausio J, Zimmermann T, Esteller M, Schotta G, Singh PB, Serrano L, Vaquero A (2017) Mammalian HP1 Isoforms Have Specific Roles in Heterochromatin Structure and Organization. *Cell Rep* 21: 2048-2057

Chen X, Barton LF, Chi Y, Clurman BE, Roberts JM (2007) Ubiquitin-independent degradation of cell-cycle inhibitors by the REGgamma proteasome. *Mol Cell* 26: 843-852

Cheutin T, McNairn AJ, Jenuwein T, Gilbert DM, Singh PB, Misteli T (2003) Maintenance of

stable heterochromatin domains by dynamic HP1 binding. *Science* 299: 721-725

Cioce M, Boulon S, Matera AG, Lamond AI (2006) UV-induced fragmentation of Cajal bodies. *J Cell Biol* 175: 401-413

Collins GA, Goldberg AL (2017) The Logic of the 26S Proteasome. *Cell* 169: 792-806

Dialynas GK, Makatsori D, Kourmouli N, Theodoropoulos PA, McLean K, Terjung S, Singh PB, Georgatos SD (2006) Methylation-independent binding to histone H3 and cell cycle-dependent incorporation of HP1beta into heterochromatin. *J Biol Chem* 281: 14350-14360

Erdel F, Rippe K (2018) Formation of Chromatin Subcompartments by Phase Separation. *Biophys J* 114: 2262-2270

Geng F, Tansey WP (2012) Similar temporal and spatial recruitment of native 19S and 20S proteasome subunits to transcriptionally active chromatin. *Proc Natl Acad Sci U S A* 109: 6060-6065

Grewal SI, Jia S (2007) Heterochromatin revisited. *Nat Rev Genet* 8: 35-46

Janssen A, Colmenares SU, Karpen GH (2018) Heterochromatin: Guardian of the Genome. *Annu Rev Cell Dev Biol* 34: 265-288

Jegou T, Chung I, Heuvelman G, Wachsmuth M, Gorisch SM, Greulich-Bode KM, Boukamp P, Lichter P, Rippe K (2009) Dynamics of telomeres and promyelocytic leukemia nuclear bodies in a telomerase-negative human cell line. *Mol Biol Cell* 20: 2070-2082

Jonik-Nowak B, Menneteau T, Fesquet D, Baldin V, Bonne-Andrea C, Mechali F, Fabre B, Boisguerin P, de Rossi S, Henriquet C, Pugniere M, Ducoux-Petit M, Burlet-Schiltz O, Lamond AI, Fort P, Boulon S, Bousquet MP, Coux O (2018) PIP30/FAM192A is a novel regulator of the nuclear proteasome activator PA28gamma. *Proc Natl Acad Sci U S A* 115: E6477-E6486

Klement K, Goodarzi AA (2014) DNA double strand break responses and chromatin alterations within the aging cell. *Exp Cell Res* 329: 42-52

Koulouras G, Panagopoulos A, Rapsomaniki MA, Giakoumakis NN, Taraviras S, Lygerou Z (2018) EasyFRAP-web: a web-based tool for the analysis of fluorescence recovery after photobleaching data. *Nucleic Acids Res* 46: W467-W472

Kowarz E, Loscher D, Marschalek R (2015) Optimized Sleeping Beauty transposons rapidly generate stable transgenic cell lines. *Biotechnol J* 10: 647-653

Lachner M, O'Carroll D, Rea S, Mechtler K, Jenuwein T (2001) Methylation of histone H3 lysine 9 creates a binding site for HP1 proteins. *Nature* 410: 116-120

Larson AG, Elnatan D, Keenen MM, Trnka MJ, Johnston JB, Burlingame AL, Agard DA, Redding S, Narlikar GJ (2017) Liquid droplet formation by HP1alpha suggests a role for phase separation in heterochromatin. *Nature* 547: 236-240

Levy-Barda A, Lerenthal Y, Davis AJ, Chung YM, Essers J, Shao Z, van Vliet N, Chen DJ, Hu MC, Kanaar R, Ziv Y, Shiloh Y (2011) Involvement of the nuclear proteasome activator PA28gamma in the cellular response to DNA double-strand breaks. *Cell Cycle* 10: 4300-4310

Li S, Jiang C, Pan J, Wang X, Jin J, Zhao L, Pan W, Liao G, Cai X, Li X, Xiao J, Jiang J, Wang P (2015) Regulation of c-Myc protein stability by proteasome activator REGgamma. *Cell Death Differ* 22: 1000-1011

Li X, Amazit L, Long W, Lonard DM, Monaco JJ, O'Malley BW (2007) Ubiquitin- and ATP-independent proteolytic turnover of p21 by the REGgamma-proteasome pathway. *Mol Cell* 26: 831-842

Lippman Z, Gendrel AV, Black M, Vaughn MW, Dedhia N, McCombie WR, Lavine K, Mittal V, May B, Kasschau KD, Carrington JC, Doerge RW, Colot V, Martienssen R (2004) Role of transposable elements in heterochromatin and epigenetic control. *Nature* 430: 471-476

Lleres D, James J, Swift S, Norman DG, Lamond AI (2009) Quantitative analysis of chromatin compaction in living cells using FLIM-FRET. *J Cell Biol* 187: 481-496

Lleres D, Bailly AP, Perrin A, Norman DG, Xirodimas DP, Feil R (2017) Quantitative FLIM-FRET Microscopy to Monitor Nanoscale Chromatin Compaction In Vivo Reveals Structural Roles of Condensin Complexes. *Cell Rep* 18: 1791-1803

Luijsterburg MS, Dinant C, Lans H, Stap J, Wiernasz E, Lagerwerf S, Warmerdam DO, Lindh M, Brink MC, Dobrucki JW, Aten JA, Fousteri MI, Jansen G, Dantuma NP, Vermeulen W, Mullenders LH, Houtsmuller AB, Verschure PJ, van Driel R (2009) Heterochromatin protein 1 is recruited to various types of DNA damage. *J Cell Biol* 185: 577-586

Ma CP, Slaughter CA, DeMartino GN (1992) Identification, purification, and characterization of a protein activator (PA28) of the 20 S proteasome (macropain). *J Biol Chem* 267: 10515-10523

Ma CP, Willy PJ, Slaughter CA, DeMartino GN (1993) PA28, an activator of the 20 S proteasome, is inactivated by proteolytic modification at its carboxyl terminus. *J Biol Chem* 268: 22514-22519

Machida S, Takizawa Y, Ishimaru M, Sugita Y, Sekine S, Nakayama JI, Wolf M,Kurumizaka H (2018) Structural Basis of Heterochromatin Formation by Human HP1. *Mol Cell* 69: 385-397 e388

Maison C, Almouzni G (2004) HP1 and the dynamics of heterochromatin maintenance. *Nat Rev Mol Cell Biol* 5: 296-304

Mao I, Liu J, Li X, Luo H (2008) REGgamma, a proteasome activator and beyond? *Cell Mol Life Sci* 65: 3971-3980

Martin C, Zhang Y (2005) The diverse functions of histone lysine methylation. *Nat Rev Mol Cell Biol* 6: 838-849

McCann TS, Tansey WP (2014) Functions of the proteasome on chromatin. *Biomolecules* 4: 1026-1044

Murata S, Kawahara H, Tohma S, Yamamoto K, Kasahara M, Nabeshima Y, Tanaka K, Chiba T (1999) Growth retardation in mice lacking the proteasome activator PA28gamma. *J Biol Chem* 274: 38211-38215

Nielsen PR, Nietlispach D, Mott HR, Callaghan J, Bannister A, Kouzarides T, Murzin AG, Murzina NV, Laue ED (2002) Structure of the HP1 chromodomain bound to histone H3 methylated at lysine 9. *Nature* 416: 103-107

Nishibuchi G, Nakayama J (2014) Biochemical and structural properties of heterochromatin protein 1: understanding its role in chromatin assembly. *J Biochem* 156: 11-20

Oda H, Okamoto I, Murphy N, Chu J, Price SM, Shen MM, Torres-Padilla ME, Heard E, Reinberg D (2009) Monomethylation of histone H4-lysine 20 is involved in chromosome structure and stability and is essential for mouse development. *Mol Cell Biol* 29: 2278-2295

Rapsomaniki MA, Kotsantis P, Symeonidou IE, Giakoumakis NN, Taraviras S, Lygerou Z (2012) easyFRAP: an interactive, easy-to-use tool for qualitative and quantitative analysis of FRAP data. *Bioinformatics* 28: 1800-1801

Rechsteiner M, Hill CP (2005) Mobilizing the proteolytic machine: cell biological roles of proteasome activators and inhibitors. *Trends Cell Biol* 15: 27-33

Saksouk N, Simboeck E, Dejardin J (2015) Constitutive heterochromatin formation and transcription in mammals. *Epigenetics Chromatin* 8: 3

Sawyer IA, Bartek J, Dundr M (2019) Phase separated microenvironments inside the cell nucleus are linked to disease and regulate epigenetic state, transcription and RNA processing. *Semin Cell Dev Biol* 90: 94-103

Schneider CA, Rasband WS, Eliceiri KW (2012) NIH Image to ImageJ: 25 years of image analysis. *Nat Methods* 9: 671-675

Schotta G, Lachner M, Sarma K, Ebert A, Sengupta R, Reuter G, Reinberg D, Jenuwein T (2004) A silencing pathway to induce H3-K9 and H4-K20 trimethylation at constitutive heterochromatin. *Genes Dev* 18: 1251-1262

Seo HD, Choi Y, Kim M, Kang K, Urano T, Lee D (2017) The 19S proteasome is directly involved in the regulation of heterochromatin spreading in fission yeast. *J Biol Chem* 292: 17144-17155

Seo HD, Kwon CS, Lee D (2018) The 19S proteasome regulates subtelomere silencing and facultative heterochromatin formation in fission yeast. *Curr Genet* 64: 741-752

Shoaib M, Walter D, Gillespie PJ, Izard F, Fahrenkrog B, Lleres D, Lerdrup M, Johansen JV, Hansen K, Julien E, Blow JJ, Sorensen CS (2018) Histone H4K20 methylation mediated chromatin compaction threshold ensures genome integrity by limiting DNA replication licensing. *Nat Commun* 9: 3704

Soderberg O, Gullberg M, Jarvius M, Ridderstrale K, Leuchowius KJ, Jarvius J, Wester K, Hydbring P, Bahram F, Larsson LG, Landegren U (2006) Direct observation of individual endogenous protein complexes in situ by proximity ligation. *Nat Methods* 3: 995-1000

Strom AR, Emelyanov AV, Mir M, Fyodorov DV, Darzacq X, Karpen GH (2017) Phase separation drives heterochromatin domain formation. *Nature* 547: 241-245

Sun L, Fan G, Shan P, Qiu X, Dong S, Liao L, Yu C, Wang T, Gu X, Li Q, Song X, Cao L, Li X, Cui Y, Zhang S, Wang C (2016) Regulation of energy homeostasis by the ubiquitin-independent REGgamma proteasome. *Nat Commun* **7:** 12497

Tardat M, Murr R, Herceg Z, Sardet C, Julien E (2007) PR-Set7-dependent lysine methylation ensures genome replication and stability through S phase. *J Cell Biol* 179: 1413-1426

Theis-Febvre N, Filhol O, Froment C, Cazales M, Cochet C, Monsarrat B, Ducommun B, Baldin V (2003) Protein kinase CK2 regulates CDC25B phosphatase activity. *Oncogene* 22: 220-232

Thiru A, Nietlispach D, Mott HR, Okuwaki M, Lyon D, Nielsen PR, Hirshberg M, Verreault A, Murzina NV, Laue ED (2004) Structural basis of HP1/PXVXL motif peptide interactions and HP1 localisation to heterochromatin. *Embo J* 23: 489-499

Trembecka-Lucas DO, Szczurek AT, Dobrucki JW (2013) Dynamics of the HP1beta-PCNA-containing complexes in DNA replication and repair. *Nucleus* 4: 74-82

van Dijk J, Bompard G, Cau J, Kunishima S, Rabeharivelo G, Mateos-Langerak J, Cazevieille C, Cavelier P, Boizet-Bonhoure B, Delsert C, Morin N (2018) Microtubule polyglutamylation and acetylation drive microtubule dynamics critical for platelet formation. *BMC Biol* 16: 116

Welk V, Coux O, Kleene V, Abeza C, Trumbach D, Eickelberg O, Meiners S (2016) Inhibition of Proteasome Activity Induces Formation of Alternative Proteasome Complexes. *J Biol Chem* 291: 13147-13159

Wilk S, Chen WE, Magnusson RP (2000) Properties of the nuclear proteasome activator PA28gamma (REGgamma). *Arch Biochem Biophys* 383: 265-271

Zannini L, Buscemi G, Fontanella E, Lisanti S, Delia D (2009) REGgamma/PA28gamma proteasome activator interacts with PML and Chk2 and affects PML nuclear bodies number. *Cell Cycle* 8: 2399-2407

Zannini L, Lecis D, Buscemi G, Carlessi L, Gasparini P, Fontanella E, Lisanti S, Barton L, Delia D (2008) REGgamma proteasome activator is involved in the maintenance of chromosomal stability. *Cell Cycle* 7: 504-512

Figure legends

Figure 1. A fraction of PA28γ and 20S proteasome localizes in heterochromatin foci.

A. Asynchronously growing U2OS-α4-GFP cells were induced for the expression of GFP-tagged α4 subunit of the 20S proteasome (α4-GFP, green) for 24 hours, then fixed and stained with DAPI (blue). Scale bar, 10 μm.

B. Asynchronous induced U2OS-α4-GFP cells (α4-GFP, green) were immune-stained with antibody raised against alpha 6 subunit of the 20S proteasome (α6), the regulatory complex PA28γ (PA28γ) and a subunit of the 19S regulatory complex (Rpt6), all in grey. Scale bar, 10 μm.

C. Asynchronous induced U2OS-α4-GFP (AS) were synchronized at the G1/S boundary by hydroxyurea treatment (HU, 10 mM, 16 hours) then released from HU-block for 2, 4 or 6 hours (R2h, R4h and R6h, respectively). Cells were subjected to GFP microscopy detection and flow cytometry analysis. Upper panel: bar graph indicates the percentage of cells presenting α4-GFP foci in the nucleus. Lower panel: bar graph representing the percentage of cells in G1, S and G2/M phases of the cell cycle, obtained by FACS analysis.

D. Induced U2OS-α4-GFP cells (α4-GFP, green) were immune-stained with anti-HP1β antibodies (grey). Merge of GFP and HP1 detection images are shown. Scale bar, 10 μm.

E. Co-immunoprecipitation of PA28γ and HP1β in asynchronous U2OS-α4-GFP cells. Induced U2OS-α4-GFP cells were lysed and subjected to pull-down with either antibody raised against PA28γ or GFP-TRAP, or the appropriate isotype control (CTL). Immunoblot of the pull-down (IP) and supernatant (SN) from whole cell extracts (WCE) were probed with the indicated antibodies.

Figure 2. HP1β interacts with PA28 and the 20S proteasome.

A. Proximity ligation assay (PLA) in U2OS cells. Control (CTL) or si-PA28γ treated cells were incubated with primary antibodies directed against HP1β and PA28γ and DNA stained with DAPI. Positive PLA signals appear as green dots and higher magnification views of a nucleus are shown (left). Scale bars, 10 μm. Quantification of PLA dots was carried out using ImageJ plugin (see Materials and Methods). Number of PLA dots per nucleus for HP1β/PA28γ interaction in control (CTL) or si-PA28γ treated cells is shown graphically (right). Data represent the means ± SD from 3 independent experiments, the number of analyzed cells is $n = 78$ and $n = 45$ in control and si-PA28γ treated cells, respectively.

B. Same as in A, except that cells were incubated with primary antibodies directed against HP1β and α4 (subunit of the 20S proteasome) (left). Scale bar, 10 μm. Number of PLA dots per nucleus for HP1β/α4 interaction in control (CTL) or si-HP1β treated cells is shown on the bar graph (right). Data represent the means ± SD from 3 independent experiments, the number of cells analyzed is $n = 48$ and $n = 46$ in control cells and si-HP1β treated cells, respectively.

C. Co-immunoprecipitation of PA28γ and HP1β in U2OS cells. Asynchronous U2OS cells were lysed and subjected to pull-down with antibody against PA28γ or the appropriate isotype control (CTL). Immunoblot of the input fractions (1/10[eme]), the supernatant (SN-IP) and the pull-down (IP-PA28γ) from whole cell extracts were probed with the indicated antibodies.

Figure 3. PA28γ controls heterochromatin compaction in mammalian cells, independently of its interaction with the 20S proteasome.

A. Immunoblot analysis of PA28γ expression level in total cell extracts from parental (WT) and knock-out for PA28γ (KO-PA28γ) HeLa[H2B-FPs] cells.

B. Left panel: FRET analysis in asynchronous parental (WT) and knock-out for PA28γ (KO-PA28γ) HeLa[H2B-FPs] cells. FLIM-FRET measurements were performed and the corresponding FRET efficiency spatial distribution is represented in a continuous pseudo-color scale ranging from 0 to 30 %. Scale bars, 10 μm. Right panel: Quantification of the FLIM-FRET compaction assay. Box and whiskers plot, the thick line represents median, the boxes correspond to the mean FRET values upper and lower of the median, with the whiskers covering the 10-90 percentile range. $n = 117$ nuclei (WT) and $n = 118$ nuclei (KO-PA28γ), **** p<0001 (Unpaired t-test).

C. Spatial distribution of the FRET efficiency (percentage) in representative WT and KO-PA28γ HeLa[H2B-2FPs] nuclei. The FRET percentage distribution is depicted in a continuous pseudo-color scale ranging from 0 to 30 %. Scale bars, 10 μm. Right panel: Mean FRET distributions graph showing distinct populations of FRET efficiency in WT and KO-PA28γ cells (blue and black curves, respectively).

D. U2OS-LacO cells were treated or not with a si-PA28γ or si-Luc, and transiently transfected with GFP-LacI construct the same day. Cells were recovered 48 hours later and proteins analyzed by immunoblotting. The relative abundance of PA28γ in the extracts was quantified with ImageJ software and normalized to Tubulin.

E. Representative fluorescence and immunofluorescence images of Z-stacks projection of U2OS-LacO cells treated as in (D) are shown. Cells were immune-stained with anti-PA28γ

(red) and DNA stained with DAPI (cyan) and GFP signal was imaging in parallel (green). Magnified views of GFP-LacI spot are shown in insets. Scale bars, 10 μm.

F. Quantitative analysis of the decompaction of the LacO array. Z-stacks images were acquired on U2OS-LacO cells treated as in (E) and the area of the GFP-LacI signal was quantified on a Z-projection using the ImageJ software (see Materials and Methods). Data represent the means ± SD from three biological repeats, numbers of analyzed nuclei with GFP-LacI spot were $n = 30$, $n = 31$ and $n = 29$ in control cells (CTL), si-PA28γ or si-Luc treated cells, respectively. ns, no significant, *** $P = 0.0002$; ** $P = 0.0013$, values were determined by Tukey's multiple comparisons test.

G. Cell extracts from parental HeLa[H2B-FPs] (WT), PA28γ knock-out (KO-PA28γ) cells and KO cells re-expressing the wild-type form (KO/KI-WT) or the ΔC-mutant (KO/KI-ΔC) of PA28γ, treated for 2 hours with 25 μM of MG132, were subjected to immunoprecipitation using anti-PA28γ antibodies. Immunoblotting of the supernatant (SN-IP) and the pull-down (IP- PA28γ) from whole cell extracts were probed with the indicated antibodies.

H. Left panel: spatial distribution of the FRET efficiency (percentage) in representative WT, KO-PA28γ and ΔC-mutant (KO/KI-ΔC) HeLa[H2B-2FPs] nuclei. The FRET percentage distribution is depicted in a continuous pseudo-color scale ranging from 0 to 30 %. Scale bars, 10 μm. Right panel: quantification of the FLIM-FRET measurements. Box and whiskers plot, the thick line represents median, the boxes correspond to the mean FRET values upper and lower of the median, with the whiskers covering the 10-90 percentile range. $n = 88$ nuclei (WT), $n = 76$ nuclei (KO-PA28γ), $n = 83$ nuclei (KO/KI-ΔC). n.s not significant, **** p<0.0001, (Unpaired t-test).

Figure 4. PA28γ acts down-stream of HP1β and its deletion affects H4K20 methylation.

A. U2OS-α4-GFP cells were transfected with either si-Luc, si-PA28γ or si-HP1β. One day later, the expression of α4-GFP was induced, and cells were recovered 48 hours after siRNA treatment. Immunostaining was performed to detect PA28γ (red) and HP1β (magenta) in cells treated with the indicated siRNAs. Representative images are shown (left). Scale bar, 10 μm. The percentage of cells with α4-GFP foci is shown in the bar graph (right). Error bars derived from 3 independent experiments represent the mean ± SD, $n > 47$ cells per condition. One-way ANOVA analysis showed a p-value $= 0.0001$ (****) for siRNA-PA28γ and -HP1β versus WT.

B. Asynchronous parental (WT) and knock-out (KO-PA28γ) U2OS cells were transiently transfected with α4-GFP. Cells were fixed 24 hours post-transfection and DNA stained with DAPI. Representative images of GFP signal (green) and DAPI staining (cyan) are shown (left). Scale bars, 10 μm. The percentage of cells with α4-GFP foci detected in both cell lines is shown in the bar graph, representing the mean ± SD from 3 independent experiments (right). Number of cells analyzed was $n > 40$ and $n > 45$ for WT and KO-PA28γ cells, respectively. Statistical significance was evaluated based on student's t-test, ***P-value < 0.001.

C. Asynchronous U2OS (WT and KO-PA28γ) cells were immune-stained with HP1β (grey) and PA28γ (green) antibodies (left). Both cell lines were transiently transfected with GFP-HP1β construct (right). Cells were fixed 24 hours post-transfection and stained with DAPI. Representative images are shown. Arrows indicate HP1β foci. Scale bars, 10 μm.

D. Representative immunoblots of whole cell extracts of U2OS (WT and KO-PA28γ) cells, using anti-H3K9me3 antibodies. Anti-histone H3 was used as loading control.

E. Immunoblots of whole cell extracts of U2OS (WT and KO-PA28γ) cells, using anti-H4K20me3 and anti-H4K20me1 antibodies. α-histone H3 was used as loading control. Graphical representation of the relative abundance of the mono-methylation (H4K20me1) and the tri-methylation (H4K20me3) marks on histone H4 normalized to histone H3. The mean ± SD is from four independent experiments.

Figure 5. PA28γ is a crucial factor for HP1β-linked heterochromatin compaction.

A. HeLa^H2B-2FPs cells (WT) were transfected with control si-Luc, si-PA28γ, si-HP1β or a mix of both siRNAs (si-PA28γ/HP1β) for 48 hours. Immunoblot analysis of PA28γ and HP1β protein levels in HeLa^2FPs following siRNA treatments were performed. Anti-Tubulin and anti-β actin antibodies are used as loading controls. The relative abundance of PA28γ and HP1β proteins was quantified using ImageJ software.

B. Quantification of the mean FRET efficiencies. Box and whiskers plot, the thick line represents median, the boxes correspond to the mean FRET values upper and lower of the median, with the whiskers covering the 10-90 percentile range. $n = 152$ (si-Luc), $n = 85$ (si-PA28γ), $n = 73$ (si-HP1β), $n = 61$ (si-PA28γ/HP1β). n.s not significant, *** p<0.001, **** p<0.0001 (Unpaired t-test).

C. Left panel: Representative images of the spatial distribution of the FRET efficiency (percentage) in representative control si-Luc, si-PA28γ, si-HP1β, or both siRNAs (si-PA28γ/HP1β) treated HeLa[H2B-2FPs] nuclei. The FRET percentage distribution is depicted in a continuous pseudo-color scale ranging from 0 to 30 %. Scale bars, 10 μm. Right panel: Mean FRET distributions graph showing distinct populations of FRET efficiency in si-Luc (blue curve), si-PA28γ (black), si-HP1β (red), or both si-PA28γ/HP1β (green) treated HeLa[H2B-2FPs].

Figure 6. Summary model for PA28γ and HP1β-linked heterochromatin compaction.

In wild-type cells, HP1β binds H3K9me3 and recruits a fraction of PA28γ-20S proteasome complexes on chromatin to facilitate H4K20 methylation and heterochromatin compaction. In the absence of PA28γ (KO-PA28γ cells), H4K20 methylation is affected but not H3K9me3, HP1β is still recruited on chromatin, but is unable to trigger its compaction.

Expanded view figure legends

Figure EV1. PIP30, a regulator of PA28γ, is present in heterochromatin foci with PA28γ-20S proteasome complexes, but does not influence HP1β/PA28γ interactions.

A. Asynchronous U2OS-α4-GFP cells were induced for the expression of α4-GFP and immuno-stained with anti-PIP30 antibodies (red). GFP (green) and merge images are shown. Arrows indicate PIP30 foci co-localizing with α4-GFP. Scale bar, 10 μm.

B. U2OS-α4-GFP cells were treated with either si-Luc or si-PIP30 and 24 hours later the expression of α4-GFP was induced. After 48 hours of siRNA treatment, cells were recovered and whole cell extracts were analyzed by immunoblotting. The relative abundance of PIP30 was quantified with ImageJ software and normalized to Tubulin (upper panel). Immunostainings were performed to detect PIP30 in induced U2OS-α4-GFP cells treated with si- Luc or si-PIP30. The percentage of cells containing α4-GFP nuclear foci is shown in the bar graph (lower panel). Error bars show the mean ± SD, duplicate experiments, $n = 270$ and $n = 328$ for si-Luc and si-PIP30 treated cells, respectively.

C. Whole cell extracts (30 μg) of parental (WT), knock-out for PA28γ (KO-PA28γ) and knock-out for PIP30 (KO-PIP30) U2OS cells used for the *is*-PLA were analyzed by SDS-PAGE and immunoblotted with the indicated antibodies (left). *Is*-PLA was carried out using primary antibodies directed against HP1β and PA28γ and DNA stained with DAPI. Representative images of parental (WT) and KO-PIP30 U2OS cells are presented (right). Higher magnification images are shown. Scale bars, 10 μm.

D. Quantification of PLA-dots was performed as in figure 2A. Number of PLA-dots per nucleus is shown on the bar graph. Data represent the mean ± SD from 3 independent experiments, number of cells analyzed was $n= 59$ (WT), $n = 40$ (KO-PIP30) and $n = 42$ (KO-PA28γ). Statistical significance was evaluated based on One-way ANOVA analysis (n.s. *P*-value and *** p< 0.0001 were obtained for KO-PIP30 and KO-PA28γ versus WT, respectively).

Figure EV2. Re-expression of WT-PA28γ in HeLa^H2B-2FPs^-KO-PA28γ restores chromatin compaction, and PA28γ-ΔC mutant does not interact with the 20S proteasome.

A. Immunoblot analysis of PA28γ expression level in total extracts from parental (WT), knock-out for PA28γ (KO-PA28γ) HeLa^H2B-2FPs^ cells and two independent clones of HeLa^H2B-2FPs^ cells knock-out for PA28γ in which wild-type PA28γ was stably re-expressed (KO/KI-WT #6, KO/KI-WT #8).

B. Spatial distribution of the FRET efficiency (percentage) in representative WT, KO-PA28γ and KO/KI-WT #6, KO/KI-WT #8 HeLa^H2B-2FPs^ nuclei. The FRET percentage distribution is depicted in a continuous pseudo-color scale ranging from 0 to 30 %. Scale bars, 10 μm. Quantification of the mean FRET efficiency. Box and whiskers plot, the thick line represents median, the boxes correspond to the mean FRET values upper and lower of the median, with the whiskers covering the 10-90 percentile range. $n = 88$ nuclei (WT), $n = 76$ (KO-PA28γ), $n = 53$ (KO/KI-WT #6), $n = 54$ (KO/KI-WT #8). n.s not significant, **** p<0.0001 (Unpaired *t*-test).

C. Whole cell extracts from parental HeLa^H2B-2FPs^ (WT), PA28γ knock-out (KO-PA28γ) cells and KO cells re-expressing the wild-type (KO/KI-WT) form or the ΔC-mutant (KO/KI-ΔC) of PA28γ. Cells were treated or not for 2 hours with MG132 (25 μM), and whole cell extracts analyzed by immunoblot using the indicated antibodies.

D. Co-immunoprecipitation of PA28γ and 20S proteasome from whole cell extracts without MG132 treatment were analyzed by immunoblotting of the pull-down (IP- PA28γ) and the supernatant (SN-IP 1/10eme) with indicated antibodies.

Figure EV3. PA28γ-depletion does not modify GFP-HP1β mobility.

Asynchronous U2OS and U2OS-KO-PA28γ cells were transiently transfected with GFP-HP1β construct. Twenty-four hours post-transfection, bright GFP-HP1β positive foci were

photobleached with 488nm laser and fluorescence intensity recovery was measured over time. The average FRAP profiles of GFP-HP1β in WT (black dots) and KO-PA28γ (red dots) cells were analysed and represented graphically; curves represented the mean ± SD from both cell lines, *n* = 25 and *32*, respectively. The half-time of recovery ($t_{1/2}$) and the mobile fraction percentage were analysed using easyFRAP tool (https://easyfrap.vmnet.upatras.gr/.) (Koulouras et al, 2018).

APPENDIX

Appendix Supplementary Methods

Proteasome Activity Assay

Proteasome peptidase activity was measured using black flat-bottom 96-well plates (Nunc) by incubating beads of immunopurified proteasome in 50 µl of activity buffer (20 mM Tris-HCl, pH 7.5, 5 mM $MgCl_2$, 1 mM ATP, 1 mM DTT, 10% Glycerol) containing 100 µM suc-LLVY-AMC, in presence or not of 25 µM MG132 (Enzo Life Science), for 20 min at 37°C. Proteasome activity was determined by the detection of the free AMC fluorescence using a FLx800 microplate fluorescence reader (excitation 380 nm, emission 440 nm, Bio-Tek Instruments.

Appendix Figure Supplementary

Figure S1. α4-GFP is incorporated into active 20S proteasomes associated to 19S regulatory complexes.

A. A cartoon representing the 20S proteasome and two members of the proteasome family. Left panel: The 20S core is formed of four stacked rings of seven subunits arranged as α7β7β7α7 barrel. The barrel contains the proteolytic active sites present on subunits β1, β2 and β5 subunits (in yellow). Right panel: two members of the proteasome family are presented. The 26S proteasome results from the association of the 20S proteasome with 19S regulatory complexes. This complex includes the Rpt6 subunit, one of the six AAA-ATPase subunits that form its base in contact with the 20S proteasome. The association of the 20S proteasome with two homo-heptamers of PA28γ forms the PA28γ-20S proteasome.

B. Whole cell extract of asynchronous U2OS-α4-GFP cells induced for the expression of α4-GFP for 24h was subjected to pull-down with GFP-TRAP beads. Total cell extract (WCE, 30 µg), pull-down (IP-GFP) and supernatant (SN-IP) were analysed by immunoblot with the indicated antibodies.

C. U20S-α4-GFP cell lysates were pull-down either with GFP-TRAP beads or antibodies raised against the Rpt6 subunit of 19S regulatory complex. Whole cell extract (WCE) and pull-downs were used for immunoblot analysis, using the indicated antibodies.

D. GFP-pull-downs from U2OS and U2OS-α4-GFP cell lysates were subjected to proteasome activity measurements using an exogenous peptide (suc-LLVY-AMC). At indicated point, an inhibitor of the 20S proteasome activity (MG132, 25 μM) was added.

E. U2OS cells, transfected (lower panel) or not (upper panel) with a vector allowing the expression of α4 without any tag protein. After 24 hours, both cell lines were immunostained with anti-alpha 4 antibodies. Representative images are shown. Scale bars, 10 μm.

Figure S2. α4-GFP nuclear foci are not due to GFP fusion.

A. Proximity ligation assay (PLA) was carried out in asynchronous U2OS cell line. Fixed cells were treated with primary antibodies directed against PA28γ (mouse monoclonal) and HP1α (rabbit polyclonal) and DNA stained with DAPI (upper panel). Number of PLA dots per nucleus in cells treated with both antibodies (CTL) or with only PA28γ antibodies (w/o anti-HP1α) is shown on the bar graph (lower panel). An higher magnification view of a nucleus is shown. Data represent the mean ± SD from 3 independent experiments, the number of cells analyzed was n = 40 and n = 41 in control cells and cells treated without primary HP1α antibody, respectively.

B. U2OS-α4-GFP cells were transfected with si-Luc, si-PA28γ, or si-HP1β. One day later, the expression of α4-GFP was induced, and 48 hours after siRNA transfection, cells were recovered. Proteins depletion was checked by immunoblotting. Total cell extracts were separated on SDS-PAGE and probed with the indicated antibodies. The relative abundance of the different proteins was quantified with ImageJ software and normalized to Tubulin.

C. Immunoblot of whole cell extract (30 μg) from asynchronous parental (WT) and KO-PA28γ (KO-PA28γ) U2OS cells, using anti-PA28γ. α-Tubulin was used as loading control.

D. Quantification of the mean FRET efficiency. Box and whiskers plot, the thick line represents median, the boxes correspond to the mean FRET values upper and lower of the median, with the whiskers covering the 10-90 percentile range.

Movie: α4-GFP foci dynamics as U2OS cells exit from mitosis and progress through cell cycle. Single plane images were taken at 10 minutes intervals.
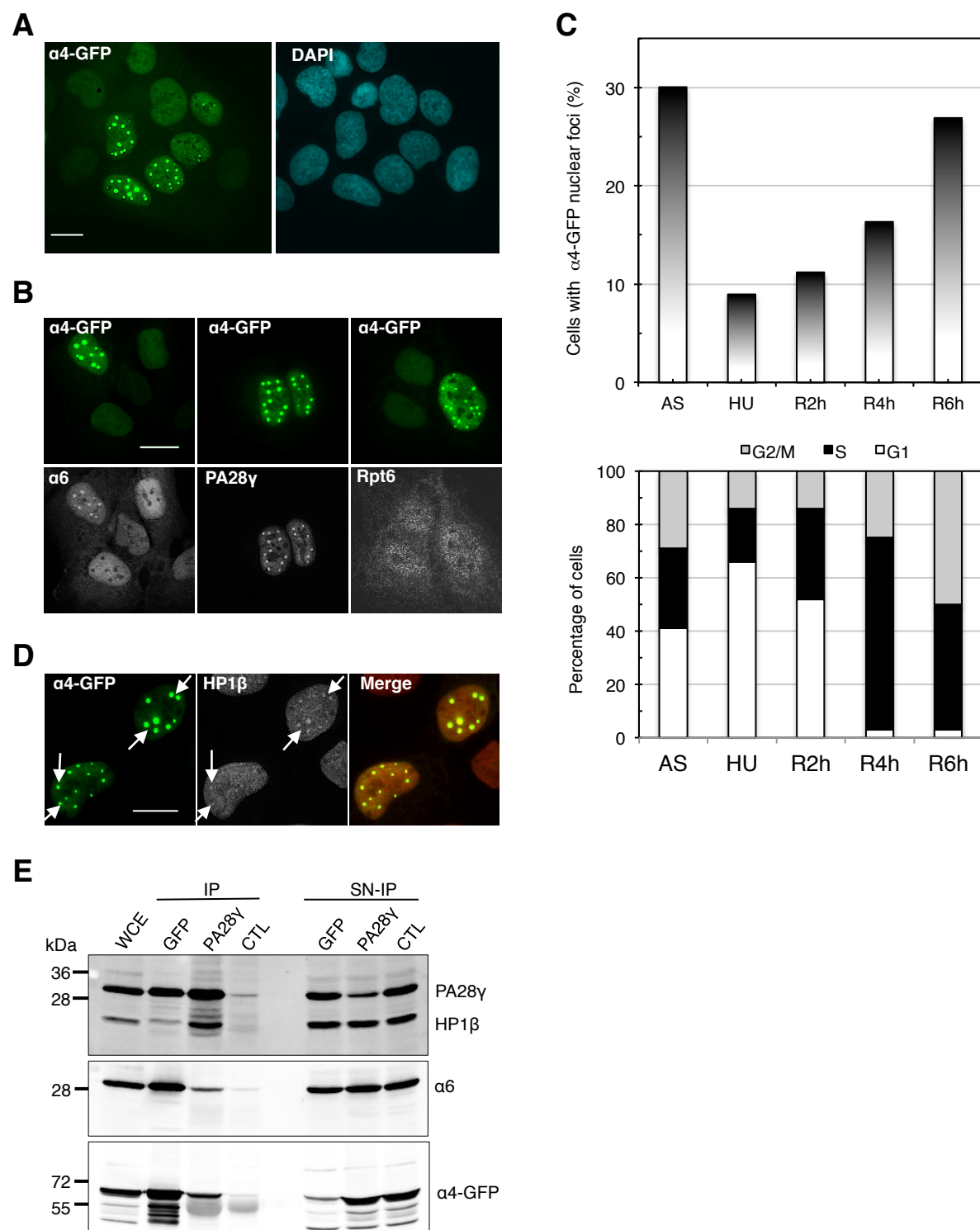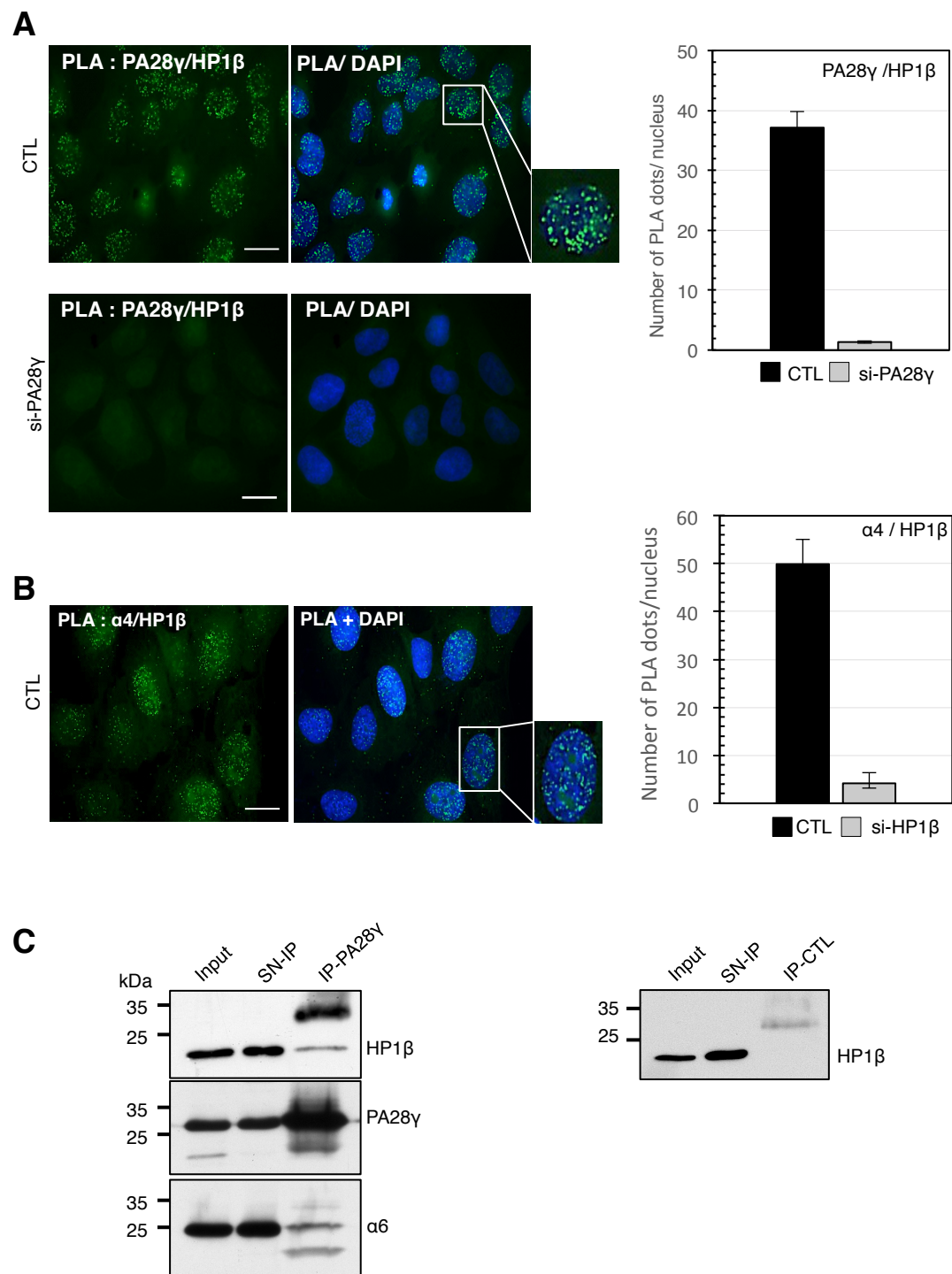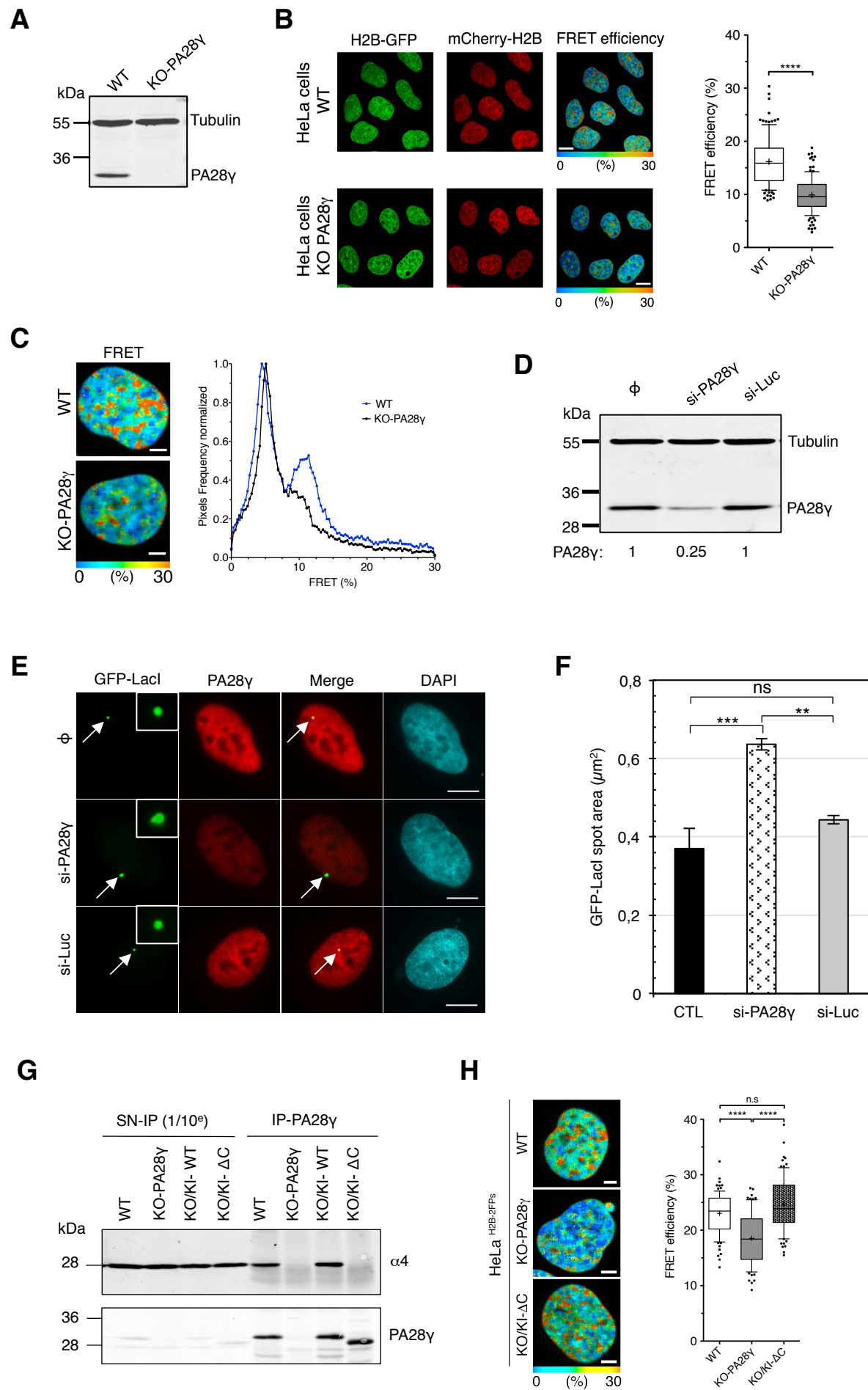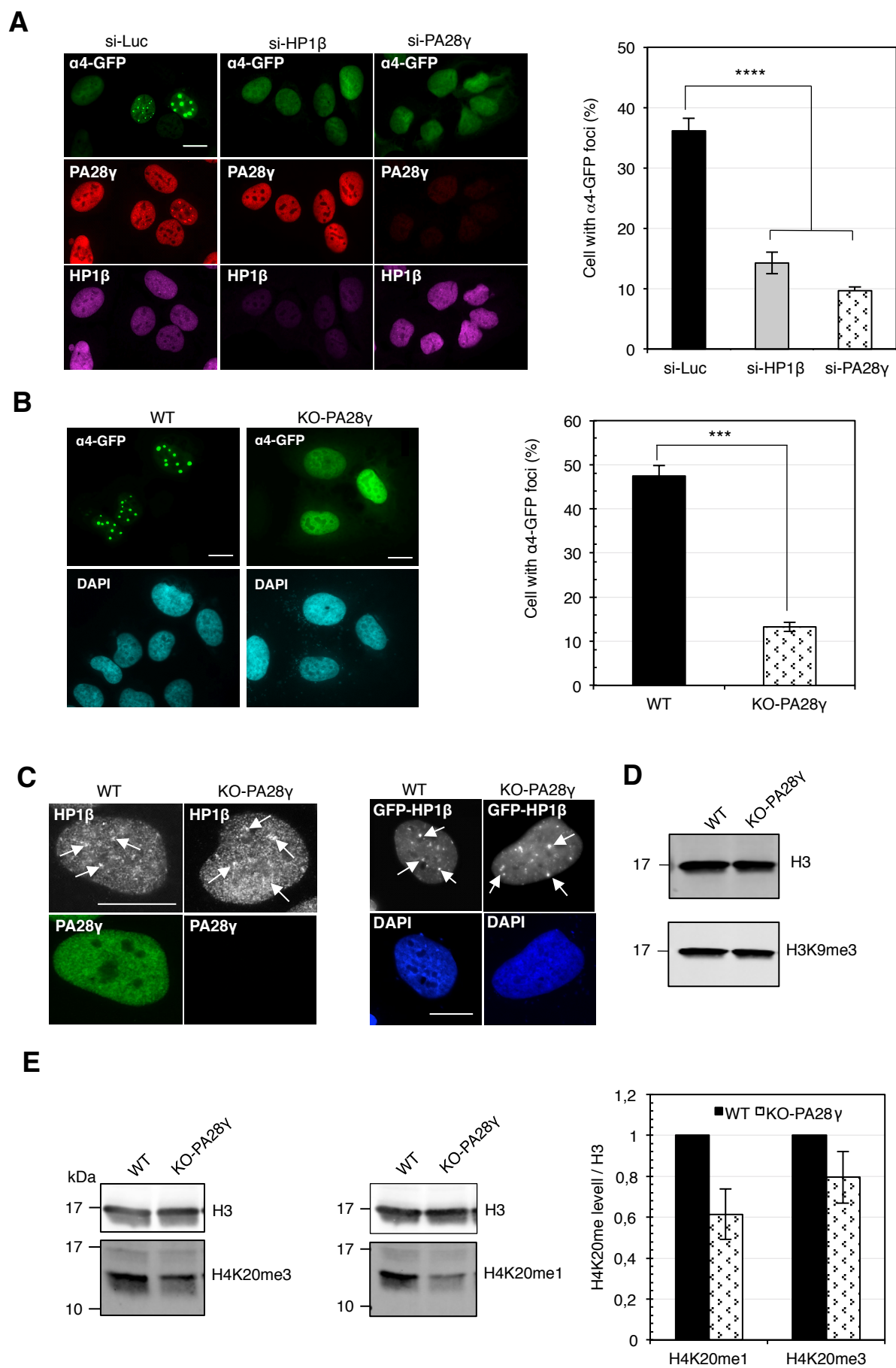
Figure 1

Figure 2

Figure 3

Figure 4
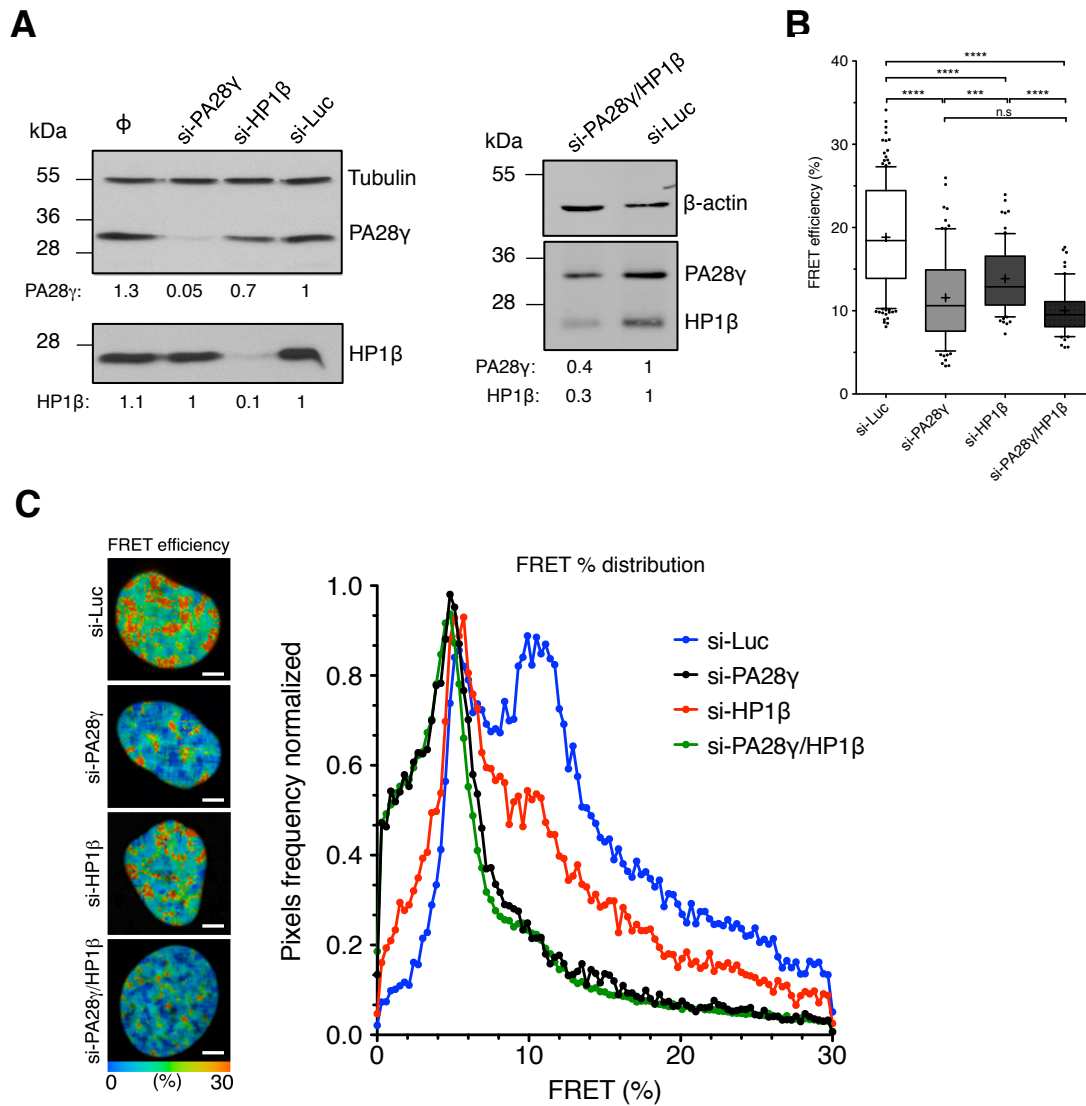
Figure 5

Figure 6

Figure EV1

A

B

WT   KO-PA28γ   KO/KI-WT # 6   KO/KI-WT # 8

FRET efficiency (%)

C

- MG132   + MG132

D

- MG132

Figure EV2

Figure EV3

Appendix Figure S1

A

B

C

D

Appendix Figure S2